Changes in aquifer properties along a seasonal river channel of the Niger Basin: identifying groundwater recharge pathways in a dryland environment

Boukari ISSOUFOU OUSMANE[a] Yahaya NAZOUMOU[a], Guillaume FAVREAU[b,d], Maman Sani ABDOU BABAYE[c], Rabilou ABDOU MAHAMAN[a], Marie BOUCHER[a,d], Ibrahim ISSOUFA[e], Fabrice M.A. LAWSON[f], Jean-Michel VOUILLAMOZ[d], Anatoly LEGCHENKO[d], Richard Graham TAYLOR[g]

[a] Département de Géologie, Faculté des Sciences et Techniques, Université Abdou Moumouni de Niamey, Niger

[b]Institut de Recherche pour le Développement (IRD), 276 Avenue de Maradi, BP 11416, Niamey, Niger

[c] Faculté des Sciences et Techniques, UMR SERMUG, Département de Géologie, Université Dan Dicko Dankoulodo de Maradi, Niger

[d] IGE, Université Grenoble Alpes, IRD, CNRS, Grenoble-INP, Grenoble, France

[e] Direction Régionale de l'Hydraulique et de l'Assainissement de Maradi (DRHA).

[f] University of Abomey-Calavi, National Institute of Water, Abomey-Calavi, Benin

[g] Department of Geography, University College London, London, UK

Highlights

- Lithological facies characterized by MRS/TDEM and borehole logs.
- Identification of previously unmapped clayey sandstone formation.
- Alluvium-bedrock architecture defined along seasonal river in the Sahel.

- Variability in hydrogeological properties controlling focused recharge identified
- Storage properties of alluvium and sandstone estimated from MRS

Abstract

In drylands of tropical Africa, groundwater plays a fundamental role in alleviating food insecurity and adapting to the effects of climate change. Substantial uncertainty persists in the renewability of groundwater resources in drylands and recharge pathways through the surface geology. Here we characterize the architecture and hydrogeological properties of alluvium and underlying sandstone and crystalline basement rocks along the ephemeral River Goulbi de Maradi in the Iullemmeden Basin of Niger using Magnetic Resonance Soundings (MRS), Time-Domain Electromagnetic (TDEM) soundings, and borehole lithological data. Considerable variations in lithological facies and hydrophysical properties are found along a series of 5 transects perpendicular to the seasonal/ephemeral river channel and adjacent plateaux of the Continental Hamadien (CH) sandstone. The CH aquifer comprises a pebbly sand facies upstream and sandstone clay facies downstream with Farak-type sandstones located at the base of the two facies. Consistent with these variations in facies, the geophysical parameters decrease from 19%, 390 ms, and 800 Ω m upstream to 3%, 160 ms, and 10 Ω m downstream, respectively for effective porosity, relaxation time, and resistivity. The transmissivity and specific yield estimated from the decline of MRS longitudinally also vary from upstream to downstream. The combined use of surface geophysics constrained by lithological borehole logs provides vital insight into groundwater replenishment in this dryland environment.

Keywords: *Goulbi de Maradi*; *Alluvium; Sandstone; Subsurface geophysics; Dryland/semi-arid; Iullemmeden Basin*

1. Introduction

In drylands of tropical Africa, groundwater is often the only perennial source of freshwater and it plays a vital role in enabling human access to safe water, livestock watering, and irrigated agriculture (Calow et al., 2010; MacDonald et al., 2012; Favreau et al., 2012; Nazoumou et al., 2016; Abdou Babaye et al., 2019). Increasingly, groundwater is also considered a source of freshwater that is more resilient to climate change than surface waters (Taylor et al., 2009; 2013; Cuthbert et al., 2019). However, in drylands where rainfall and surface water are limited, intensive use of groundwater, especially for irrigation, risks groundwater depletion (Siebert et al., 2010; Wada et al., 2010; 2012; Scanlon et al., 2012; Taylor et al., 2013; Bierkens & Wada, 2019; Jasechko & Perrone, 2021). Thus, understanding mechanisms of groundwater renewal, as well as estimating hydrogeological properties, can inform sustainable use of groundwater (Descloitres et al., 2013; Kemgang Dongmo et al., 2019).

Many aquifers in drylands are replenished by focused recharge via the infiltration of seasonal rivers or ponds (Scanlon et al., 2006; Favreau et al., 2009; Villeneuve et al., 2015; Cuthbert et al., 2016; 2019; Seddon et al., 2021). Such recharge pathways are known to be controlled by the structure and hydraulic properties of the surface geology (Scanlon et al., 2006; Wheater et al., 2010). For example, it has been widely demonstrated that the recharge rates linked to transmission losses of rivers are less influenced by river stage height than the lithology and the hydraulic conductivity of the riverbed and the unsaturated zone (Carter & Alkali, 1996; Dahan et al., 2008a; Costa et al., 2012; Flinchum et al., 2020; Zarate et al., 2021)

The application of surface geophysical methods has proven to be effective in identifying and estimating the physical properties of aquifers. Magnetic Resonance Soundings (MRS) can be used to quantify the transmissivity, permeability, and specific yield reliably at an average depth of 100

m, based on the measured effective porosity and relaxation times (Boucher et al., 2009; Vouillamoz et al., 2014). Compared to hydraulic testing, which require construction of a pumping well and monitoring piezometer, MRS is rapid, less costly, and applicable at several sites (Gev et al., 1996; Legchenko et al., 2002; Vouillamoz et al., 2008, 2014; Boucher et al., 2009; Behroozmand et al., 2015). Additionally, for sedimentary aquifers and weathered basement aquifers, it has the advantage of removing the fundamental uncertainty related to the utilization of the equivalent resistivity between groundwater and lithology (Goldman et al., 1994; Legchenko et al., 2009). MRS is vulnerable to the influence of external signals created by electrical power-lines, electrical generators, radio transmitters, cars and trains, electrical fences, and magnetic storms.

The combination of MRS and resistivity measurements such as Time-Domain Electromagnetic Method (TDEM) has a distinct advantage in that they increase the estimation of MRS parameters (e.g. effective porosity and the decay times T_1 and T_2^*), which depend on the structure and grain size of the volume investigated, respectively (Schirov, et al., 1991; Legchenko et al., 2002). For large unconfined aquifers in the Sahel including southwestern Niger and the Lake Chad Basin, this combination of methods has been used successfully to provide an estimate of aquifer properties (Boucher et al., 2009, 2012; Descloitres et al., 2013); these methods have also been applied to map freshwater-saltwater interfaces (Kafri & Goldman, 2005; Legchenko et al., 2009; Vouillamoz et al., 2012). Here, we apply a combined MRS-TDEM geophysical approach with borehole lithological logs to characterize the hydrogeological setting/recharge pathways: (1) to determine the hydrogeological properties of aquifers, (2) to define the geometry of aquifers alluvial and the Continental Hamadien (CH), and in order (3) to assess their hydraulic interconnection.

2. Study area

2.1. Location, human and hydroclimatic context

The study area, located in the southeastern edge of the Iullemmeden Basin in West Africa (Fig. 1a-b), is the River Goulbi de Maradi Basin (RGMB) (Fig. 1c). This region is one of the most densely populated areas in Niger (81 to 105 inhabitants/km^2) and a fertility rate of 7.6 children per woman that is among the highest rates in the world (INS, 2012). People in this region depend mainly on rain-fed agriculture and animal husbandry, which have recently become less productive and increasingly vulnerable to climate hazards. During drought years, declines in agricultural production have led to major food crises and occasionally famines (Nazoumou et al., 2016).

The River Goulbi de Maradi (RGM), the only ephemeral source of surface water, drains a transboundary river basin between the Republic of Niger and the Federal Republic of Nigeria. Its flow is seasonal, occurring episodically from July to October depending on local rainfall and releases from the Jibya dam in northern Nigeria (storage capacity: 142 million m^3). The headwater area of the river in northern Nigeria is underlain by crystalline massifs of Zamfara, under River Gada in Nigeria, and crosses 120 km into Niger to join Sokoto Rima, a tributary of the Niger River (ORSTOM, 1972). In Niger, the RGM has a watershed area of 6650 km^2, comprising ~65% of the total basin area (10326 km^2).

The RGM basin currently experiences a semi-arid climate where two masses of air circulate: the monsoon (hot and humid) coming from the Atlantic Ocean and delivering rainfall from June to September and harmattan (dry and very hot) coming from the Sahara desert to the north (Issa Lélé & Lamb, 2010). The synoptic meteorological station at Maradi airport recorded mean annual rainfall of 520 mm with a standard deviation of 120 mm from 1953 to 2014. Ambient daily air temperatures vary from 25 to 40°C for periods of high and low temperature, respectively; mean annual potential evapotranspiration is ~2000 mm.

2.2. *Geology and hydrogeology*

The geology of the study area consists of Quaternary formations, the Continental Hamadien (CH) of the Upper Cretaceous, and the crystalline to crystallophyllian Precambrian basement (Fig. 1c). The Precambrian basement, which consists of granites, gneisses, and schists from Paleoproterozoic to Cambrian, is exposed in the southern part of the study area along the Nigerian border in an east-west direction. It is in geological continuity with the northern Nigerian shield mobile zone (Mignon, 1970). Outcrops are isolated from each other either by Quaternary deposits (dune or alluvial sands) or by conglomerate sandstone from the Upper Cretaceous (CH). Tectonic events affecting the area are marked by pan-African ductile deformations with a major orientation NW-SE to E-W (Mignon, 1970). Due to limited weathering and regolith thickness, crystalline rock (basement) aquifers of the area produce low well yields (0.5 to 3 m^3/h). To source water, the people who live on these formations dig shallow wells by hand in the sediments of ephemeral rivers.

The Continental Hamadien (CH) constitutes a continental formation that has been formed in parallel to marine sediments deposited during various transgressions during the Upper Cretaceous (Dikouma, 1990). Surmounted by Quaternary deposits including dune sands on the plateaux and alluvial deposits in the valleys, the CH is composed of two geological groups specifically: a pebbly sand series at the top and Farak-type sandstones at the base with often-thin clayey intercalations. The pebbly sand series is characterized by the presence of rolled quartz pebbles with grain sizes of 20 to 30 mm but can be as coarse as 60 to 70 mm comprising an abundance of slightly worn quartz, and kaolinized feldspars (Greigert, 1966). This formation occupies large northeastern depressions, between longitudes 7° and 8°, dug in Farak-type sandstones during erosion phases of the Upper Cretaceous. Farak-type sandstones are clayey with the presence of worn quartz exceptionally reaching 1 to 2 mm, most often embedded in a whitish kaolinitic paste. The thickness and lateral

extent (geometry) of these different formations have not, however, been well reported. In the Nigerian part of the Iullemmeden basin, the CH is represented by the Rima Group formation (Toyin et al., 2016).

Hydrogeologically, the CH constitutes a transboundary aquifer between Niger, Nigeria, and Mali (OSS, 2008). It is found throughout the study area in Niger except for the southern part and forms an unconfined aquifer. Recorded well yields vary spatially from 8 to 70 m^3/h. Quaternary formations comprise aeolian sands encountered on the plateau and alluvium found along with the RGM and its tributaries. The thickness of the alluvium ranges from 10 to 30 m and derives from the erosion of CH and Precambrian basement (BRGM, 1978; Durand et al.,1981). At present, the alluvial aquifer is used much more for irrigation compared to the CH. Static water levels in the alluvium vary from 4 to 18 m; pumping rates are 20 to 70 m^3/h (Issoufou Ousmane, 2014).

3. Materials, data, and methods

Our methodological approach (Fig. *2*) comprises an analysis of borehole records, piezometric measurements, and geophysical measurements (MRS and TDEM).

3.1. Borehole records and piezometric measurements

Well records from ~500 boreholes that were drilled between 1980 and 2015 and range in depth from 20 to 300 m, were amassed from the Maradi Regional Direction of Hydraulics and Sanitation (DRH/A-Maradi). These well records comprise lithological logs, an equipment plan, and static water level depths. Records with missing data were discarded. For the boreholes showing erroneous data, lithological descriptions were corrected based on neighboring lithological logs. Five transects perpendicular to the RGM (Fig. 1c) were then chosen for MRS and TDEM experiments. Under this research, eight additional dedicated piezometers were constructed to assist in the

characterization of the superficial geology and refine the interpretation of geophysical parameters: resistivity, effective porosity, and decay times T_1 and T_2^*. Further, we considered field measurements of static water levels in 165 wells and boreholes, measured in October 2019. Based on these data, which were leveled using a Digital Elevation Model (DEM) of 30 m resolution (https://www2.jpl.nasa.gov/srtm/), piezometric contours were initially drawn by kriging (Surfer) and then reworked in ArcGIS to correct erroneous interpolations related to DEM artifacts.

3.2. Time Domain electromagnetic (TDEM) soundings

TDEM is an electromagnetic method used to determine the electrical resistivity of rocks as a function of depth employing diffusion of a transient electromagnetic field in the time domain (Descloitres et al., 2013). For hydrogeological studies, resistivity is associated inversely with one or more of effective porosity, electrical conductivity, clay content, and substrate texture (Kafri & Goldman, 2005; Descloitres et al., 2013). For non-argillaceous rocks completely saturated with water, resistivity can be obtained from equation (1) defined by Archie, (1941):

$$\rho_w/\rho_r = a\theta^m \quad (1)$$

where ρ_w water resistivity; ρ_r rock apparent resistivity; θ rock porosity (or water content at saturation); a and m are empirical parameters dependent on geology. Their values are respectively close to 1 and 2 (Kafri & Goldman, 2005).

TDEM emits an electric current from the surface using a transmission cable, which, being constant and periodic, produces a primary magnetic field. It results in a variation of the magnetic field that induces an electromotive force (emf) in the medium traversed following a sudden cut in the power supply. The emf generates an electric current, the eddy current, whose circulation lines describe a geometry similar to that of the transmission loop (Nabighian and Macnae, 1991). The

gradual decrease in the intensity of the electric current emitted due to the resistivity of the formations traversed causes a voltage pulse, which produces streams of the current induced at a greater depth and distance from the transmission loop. This process creates a secondary magnetic field measured at the surface through a receive loop (R_x), which may be the same transmit loop (coincident shape-loop) or a smaller loop either centered in the transmit loop (central shape-loop) or away from the center (offset shape-loop).

In this study, TDEM measurements were carried out using the TEM FAST 48HPC equipment (Applied Electromagnetic Research Technology, www.aemr.net). Three field campaigns took place in January and August 2019 as well as April 2020. During these campaigns, 31 TDEM soundings (Fig. 3a) were performed near boreholes or piezometers and following the transects perpendicular to the RGM (Fig. 1c). Square loops at variable sizes (150, 100, and 50 m), configured with coincident mode (150 x 150, 100 x 100, and 50 x 50 m^2) and in a central mode (150 x 50 m^2), were used.

TDEM data were inverted individually using TEM-RESEARCHER, TEM-RES software (www.aemr.net, 2005; Barsukov et al., 2015) similarly to Boucher et al. (2009). The first step consists of eliminating outliers at the start of the curve (i.e. distortions automatically eliminated by the software) or the end (i.e. background noise). The sounding of the 50 x 50 m^2 coincident loop is then reversed to determine the model of the first terrain which, in turn, is fed into the central 150 x 50 m^2 loop to find the deep terrain model. The deep terrain model is useful for correcting the first terrain model. These two models are then used to interpret the sounding of the coincident loop 150 x 150 m^2. The result is acceptable if a single resistivity model is obtained that matches the three soundings with low RMS values, < 3%.

3.3. *Magnetic Resonance Sounding (MRS)*

The basic principles of (proton) Magnetic Resonance Sounding (MRS) are explained in Legchenko and Valla (2002) and Behroozmand et al. (2015). Proton magnetic resonance, sometimes known as surface nuclear magnetic resonance (SRMN), uses an alternating magnetic field to excite protons in water molecules. In principle, in the equilibrium state (i.e., without excitation), protons of each water molecule are oriented in the same direction as the Earth's magnetic field B_0, the local static field that prevails in an area. Protons deviate from their original position as the result of the creation of a secondary magnetic field due to the emission of the alternating current signal at a specific frequency or Larmor frequency defined by equation (2):

$$f_L = \frac{\gamma_p}{2\pi} B_0 \qquad (2)$$

where B_0 (Tesla) is the Earth's magnetic field which prevails at the measurement point; γ_p the proton's gyromagnetic ratio.

After the power to this secondary magnetic field is cut, protons precessing at the same frequency return to equilibrium and release energy as a signal of magnetic field relaxation. Detected by the reception loop (R_x), this magnetic relaxation field indicates the presence of effective porosity (free water content) in the medium crossed. The derivable parameters of this signal include effective porosity and relaxation time constants, T_1 and T_2^* depending on the mean size of the water-saturated pores, as a function of the depth (Legchenko et al., 2004). However, estimation of T_2^* decay time can be affected by the host rocks magnetic heterogeneity (Legchenko and Valla, 2002; Vouillamoz et al., 2011); T_1, which is not very sensitive, offers the best choice, especially in sedimentary environments with a strong MRS signal (Boucher et al., 2009; Descloitres et al., 2013). For MRS, we employed NUMIS^{Plus} and NUMIS^{Lite} (www.iris-instruments.com) instruments and a

proton magnetometer for measuring the magnetic field. During three campaigns in 2019 and 2020, 19 MRS were also carried out near boreholes or piezometers and along transects perpendicular to the River GM (Fig. 1c).

The characteristics of all soundings are summarized in Table 1. Two kinds of transmitter-receiver loop geometries, both configured in coincident mode, were mainly used: a 150 x 150 m^2 square shape-loop (for 4 MRS) and two eight shape-loop 100 x 100 and 50 x 50 m^2 (for 11 and 2 MRS, respectively). Two MRS were carried out with an eight loop of 75 x 75 and 37.5 x 37.5 m^2, respectively. To optimize investigation depth, a strong pulse moment between 6500 and 13000 A.ms was injected with Numis^{Plus} (Behroozmand et al., 2015; Legchenko et al., 2018). For Numis^{Lite}, the low resistance of the loop did not allow more than 1500 A.ms to be injected for an eight-loop configuration of 100 x 100 m^2. However, by reducing the loop size to 50 x 50 m^2 and doubling the cable, the pulse moments were optimized to 5000 A.ms. The maximum amplitude of the signal is between 1253 and 165 nV (Fig. 3b). In the study area, the daily variation of Larmor frequency is from 8:30 am to 1 pm and from 2 to 6 pm where an ascent and descent can be observed, and stability of the frequency from 6 pm until 8 am. It has been indicated that the daily variations of frequency are linked to sun activity (Vouillamoz et al., 2008).

MRS data were inverted with SAMOVAR_V11.6 software using 04 °N like magnetic field inclination for all the sites; linear filters were established based on the resistivity models defined by the TDEM (Behroozmand et al., 2012; Legchenko et al., 2018). For each sounding, we realized two inversions. A smooth automatic inversion to obtain effective porosity (water content) distribution and decay times (Descloitres et al., 2013) and a block inversion with one layer for the soundings outside of the valley and at two layers for the soundings in the valley to obtain average values for the effective porosity and the decay times T_1 and T_2^*. To assess the quality of soundings,

we compared the generator frequency (invariable during the day) to the Larmor frequency for each given site (Legchenko et al., 2016). Thus, for all the soundings, the difference in frequency was less than 1.5 Hz (Δf), and the signal/noise ratios (S/N) vary between 29.5 and 6.6 except the Nielloua_GF02 and Kartakaye presenting respective values of 4.6 and 2.8 (Table 1). MRS are of good quality if the ratio S/N is >2 and Δf < 2 Hz (Lubczynski & Roy, 2005; Legchenko, 2007; Descloitres., 2013).

3.4. Hydrodynamic parameters estimation

3.4.1. Hydrodynamic parameter estimation from pumping tests

Two constant-discharge pumping tests were conducted on the drinking water supply boreholes in Hanou Gazane and Nielloua (green point, Fig. 1c) proximate to MRS and TDEM experiments) in August 2019 at rates from 8.9 and 10.2 m^3/h for 7 and 6 h, respectively. Although it was not possible to measure drawdowns on the pumping boreholes, observation piezometers located less than 20 m from the pumped boreholes were monitored using pressure transducers (InSitu Rugged Troll 100) that recorded groundwater levels every minute during drawdown and recovery. Measured drawdowns of 1 and 0.38 m were recorded; pumping was stopped and recovery was recorded for 4.6 and 18 h, respectively. Further, existing data from 4 pumping tests of 20 to 48 h in duration, carried out in water supply boreholes were provided by the Regional Directorate of Hydraulics and Sanitation of Maradi (DRH/A). The characteristics of all pumping tests are summarized in Table 2.

Pumping tests were interpreted using the Cooper & Jacob (1946) method, based on the graphical estimation of transmissivity and storage coefficient or drainage porosity for unconfined aquifers. However, due to the low reliability of this method to estimate the storage coefficient, only

the transmissivity was calculated, through the equation (3) (Meier et al.,1998; Sánchez-Vila et al., 1999).

$$T = \frac{2.3}{4\pi} \times \frac{Q}{\Delta S} \quad (3)$$

where T (m^2/s) the transmissivity; Q (m^3/s) the pumping rate; ΔS (m) is the slope for a logarithmic cycle; *tc* (s) the time corresponding to the abscissa of a point of intersection of the asymptote at the depth line with zero pressures. The choice of this method has been motivated by the simplicity of the sites: homogeneous aquifers that are generally unconfined, and the pumped well has an infinitesimal diameter.

To estimate hydrodynamic parameters from MRS data requires *a priori* establishment of a calibration coefficient (C_p) with borehole data (Legchenko et al., 2004; Plata and Rubio, 2008; Vouillamoz *et al.*, 2008, 2015; Boucher *et al.*, 2009). As time T_1 is linked to the mean size of pores that contain groundwater (Schirov, et al., 1991; Legchenko *et al.*, 2002), hydraulic conductivity (K_{MRS}) can be computed from equation (4) and transmissivity (T_{MRS}) multiplied by the saturated thickness (ΔZ) through equation (5) (Legchenko et al., 2002):

$$K_{MRS} = C_p \theta_{MRS} T_1^2 \quad (4)$$

$$T_{MRS} = K_{MRS} \times \Delta Z = C_P \theta_{MRS} T_1^2 \times \Delta Z \quad (5)$$

where T_{MRS} the transmissivity (m^2/s), K_{MRS} the hydraulic permeability (m/s), C_P is the Parameterization coefficient depending on the nature and structure of the geological medium, θ_{MRS} the effective porosity (%), T_1 the decay time (ms), and ΔZ the thickness of the saturated layer.

As parameters provided by MRS directly relate to the hydrodynamic properties of the aquifer, the calibration coefficient C_p can be estimated by the following relationship:

$$C_p = T_{pumping} \div \theta_{MRS} T_1^2 \quad (6)$$

For areas where pumping tests and MRS measurements exist, (Legchenko et al., 2002) proposed the following formula:

$$C_p = \sum T_{Pumping} \div \sum \theta_{MRS}\, T_1^2 \quad (7)$$

Additionally, the specific yield ($S_{y(MRS)}$) can be estimated by the MRS data. In this sense, several relationships between the specific yield and the MRS effective porosity have been developing. For example, Vouillamoz *et al.*, (2005) proposed the following relationship:

$$S_{yMRS} = C_y \times \theta_{MRS} \quad (8)$$

where $S_{y(MRS)}$ is the specific yield estimated by MRS; θ_{MRS} the MRS effective porosity and C_y a parametric factor that depends on geology.

4. Results

4.1. Description of the lithological facies from drilling

Fig. 4 shows lithological logs along the upstream-downstream transect, the presence of pebbly sand series, and Farak-type sandstones described in section 2.2. The pebbly sand series is found in the upstream part, delimited from the contact area by the outcrop of basement rocks in the south to Souloulou, ~25 km north-west of Maradi. Its thickness varies from a few tens of meters to more than 60 m. Farak-type sandstones constitute the basic formation encountered throughout the study area. They are lithologically fine to medium sandstones, clayey or silty, which appear to be in direct contact with the Precambrian basement. The thickness of these sandstones varies from 50 to over 300 m, as shown by the exploration borehole (PK-374.5 at Guidan Roumdji, Fig. 4). Downstream, we identify a new, previously unmapped formation of finer, clayey texture, defined as the clay-

sandstone series. It is composed of compact clays, sandstone clays, and clayey silts. Its lateral extension goes from before Koumchi, where its thickness is between 15 to 25 m, to Souloulou where its thickness is about 80 m.

4.2. TDEM and MRS associations with hydrolithologies

Fig. 5 depicts the outcomes of MRS and TDEM experiments with borehole lithological logs of Guidan Kaji (GK) (Maradi city) (Fig. 5a) and Djirataoua_GF01 piezometer (Djirataoua site) (Fig. 5b). The TDEM station is located ~500 m from the borehole GK, drilled in 2015 to a depth of 237 m in the unaltered granite basement at 235 m. The resistivity model established from TDEM is well correlated to borehole lithological descriptions. Within the CH, a resistant formation (800 Ω m) from 0 to 55 m corresponds to the pebbly sand series; a conducting terrain (9, 17 and 6 Ω m) from 57 to 68, 68 to 150 and from 150 to 240 m corresponds to the Farak-type sandstones. Finally, a very resistant terrain (2000 Ω m) corresponds to unaltered granite basement at 240 m.

The Djirataoua borehole is installed mainly within alluvium and most shallow horizons of the CH to a depth of 45 m (Fig. 5b). The MRS and TDEM stations are located ~400 m from this borehole. Well logs show clayey alluvium from a depth of 0 to 5 m with resistivities of 15 Ω m, sandy-gravel from 5 to 26 m, and CH pebbly sand series from 26 to 42 m, both with a resistivity of 57 Ω m. From 49 to 140 m, TDEM shows a conducting terrain (10 Ω m) corresponding to Farak-type sandstones that is underlain by a very resistant formation corresponding to the unaltered granite basement. In addition, the MRS confirmed the presence of the fine and coarse alluvium with an average effective porosity of 19% and a decay time T_1 of 260 ms (Fig. 5b). In the lower part, from 26 to 49 m and from 49 to 140 m, corresponding respectively to the pebbly sand series and Farak-type sandstones, the measured value of effective porosity average and T_1 time are respectively 17% and 260 ms.

Spatial and vertical variations in electrical resistivity have made it possible to define resistivity ranges for each geological formation as defined in Fig. 4. Minimum and maximum values are between 12 and 300 (Ω m) for alluvium, 22 and 800 (Ω m) for the pebbly sand series, 10 and 43 (Ω m) for the clay-sandstone series, 6 and 17 (Ω m) for the Farak-type sandstone, and 2000 (Ω m) for the Precambrian basement. Mean and median values and standard deviations from the statistical analysis are summarized in Table 3.

Similar to TDEM, MRS results are reported by geological formation (Table 4). Over the entire study area, values measured for the alluvium range from 7 to 20% for effective porosity and 220 to 300 ms for mean decay times (T_1). For CH formations, values are reported as a function of spatial variations in hydrolithological facies. In the upstream part (Fig. 4) represented by pebbly sand series and Farak-type sandstones, values measured for mean effective porosity and decay times T_1 are between 11-18% and 220-390 ms. Downstream, the clay-sandstone series and Farak-type sandstones have lower values ranging from 3 to 11% for effective porosity average and 220-300 ms for the T_1 average. Mean and median values and the standard deviation for statistical analysis are also given in Table 4.

4.3 Estimation of hydrodynamic parameters

Estimated transmissivities from pumping tests range from 1.4×10^{-3} to 2.2×10^{-2} m^2/s. For the boreholes with observation piezometers, low storage coefficients (7.9×10^{-3}, 5.6×10^{-4}) are calculated; detailed results are given in Table 5. In the area with weakly weathered crystalline rocks, boreholes were installed strictly in the alluvium; MRS soundings show that the aquifer consists mainly of alluvium whereas the rocks of the underlying basement are dry (Fig. 6a). As all boreholes and MRS are limited to the sedimentary sequences, one calibration factor was employed

355 across the entire study area based on transmissivity values (i.e., 2.2 x 10^{-2}, 4.7 x 10^{-3}, and 1.4 x 10^{-3} m^2/s), obtained from pumping tests (Table 5).

357 In the study area, the C_p values obtained vary from 0.3 x 10^{-8} to 4.5 x 10^{-8} $m/s/ms^2$. An average
358 value of 2.2 x 10^{-8} $m/s/ms^2$ was calculated by applying equation (8). The C_p value is very similar
359 to that computed/observed by Boucher et al., (2009) for the Continental Terminal aquifers in the
360 south-western part of Niger (C_p = 1.4 x 10^{-8} $m/s/ms^2$). This favorable comparison is reasonable
361 considering that the two geological contexts are continental, and they constitute sandy-gravelly
362 aquifers. Considering this lithologic similarity, a common C_y is used (0.38) to estimate the MRS-
363 specific yield. The obtained values of transmissivity (T_{MRS} in m^2/s), permeability (K_{MRS} in m/s), and
364 specific yield ($S_{y(MRS)}$ in %) are given in Table 6.

365 *4.4 upstream-downstream transects*

366 Fig. 6 shows MRS, TDEM, and borehole lithology results, from upstream to downstream,
367 represented with the topography on the different transects. On transect 1 (Fig. 6a), it is notable that
368 the geological nature of the weakly weathered granite basement near the surface did not allow for
369 the interpretation of TDEM measurements. MRS results indicate that the alluvial aquifer has a
370 maximum thickness of ~15 m with mean effective porosity of 18, 13, and 9%, and T_1 values of
371 220, 200, and 230 ms respectively for GF01, GF02, and GF03. Consistent with the lithological
372 description of the boreholes, these values may suggest that the aquifer is composed of fine to
373 medium-grained materials (Legchenko et al., 2009). The results show that the distribution of
374 effective porosity along this transect can be interpreted by the local lithological composition of
375 each station. The effective porosity is much higher, 18%, at GF01 station, which is located 50 m
376 from the river bed, where the lithology is sandy. In contrast, due to the low thickness of the aquifer

(~ 6 m), low effective porosity (9%) is observed at GF03 station also localized at 50 m from the minor river bed (Fig. 6a).

On transects 2 and 3 (Fig. 6b-c), the configuration of the effective porosity distribution illustrates two aquifers in hydraulic continuity in the valley. The upper aquifer corresponds to the alluvial aquifer and is identified in the shallowest 26 m with a saturated thickness from 8 to 26 m for GF01 and GF02 stations (Fig. 6b). The relative average value of effective porosity is 19%, the resistivity is between 12 and 57 Ω m, and the average T_1 time is 260 ms. On transect 3 (Fig. 6b), the alluvial aquifer located between 6 and 30 m is characterized by relatively low average values, 5 to 17%, 240 ms, and 25 to 40 Ω m respectively for effective porosity average, time T_1, and resistivity, relative to the previous transect. The lithologic composition consists of fine to medium clayey sands and sandy clay devoid of coarse elements, which is in good agreement with the values of T_1.

On transects 2 and 3 (Fig. 6b-c), the deeper aquifer within Continental Hamadien formations are identified through the borehole lithologies and TDEM soundings, that the pebbly sand series is located at the base of Quaternary deposits of alluvium and dune sands (Fig. 6b-c). The resistivity of this layer varies from 23 to 180 Ω m; effective porosity values are between 9 to 17%, and the T_1 time is from 250 to 490 ms. Collectively these observations indicate relatively fine to coarse deposits such as sands, sandstones, and gravels with conglomerates. Along both two transects, it was noted that the presence of a low resistivity layer (10 Ω m on average) was composed of clayey or silty sandstone or Farak-type sandstones (CH). On transect 2 (Fig. 6b), this layer rests on the Precambrian crystalline basement with a high resistivity of 2000 Ω m but presents effective porosity of 7 to 15% and the T_1 of 240 to 350 ms a little lower compared to pebbly sand series.

Along transects 2 and 3 shown in (Fig. 6b-c), the alluvial aquifer is also present along transects 4 and 5 at 25 to 30 m depths comparable to the previous transects (Fig. 6d-e). This aquifer is characterized by a saturated thickness of 12 to 15 m; static water levels are between 14 and 17 m. However, in this part of the basin, geophysical and lithological evidence suggests that the alluvium is progressively becoming finer (more clayey) thereby reducing its transmissivity and effective porosity. Despite similar resistivity values ranging between 10 and 43 Ω m along both transects, the free effective porosity and T_1 vary; 8 to 10 and 3 to 6% for free effective porosity, and T_1 from 190 to 230 and 120 to 180 ms for transects 4 and 5, (Fig. 6d-e), respectively. These observations support the basic principle that the decrease in grain size and increasing clay content lead to a decrease in T_1 (Legchenko et al., 2009).

Geophysical and lithological results along both two transects for the underlying CH aquifer reveal the absence of pebbly sand series and confirm the presence of clay-sandstone series with a low resistivity value between 10 and 43 Ω m. The borehole's lithology is composed of clay mixed with fine to medium elements, such as sands, sandstones, and silts. This predominantly clayey series is also characterized by low effective porosity (3 to 10%) and T_1 times (160 to 280 ms). However, it seems that Farak-type sandstones present the same geophysical characteristic, as indicated by the mean values of resistivity (~ 11 Ω m) and time T_1 of 180 and 250 ms despite the decrease in the effective porosity (5 to 8%).

4.5 Groundwater flow pattern

As demonstrated in the previous section, the depth profiles of effective porosity (water content) obtained by MRS do not show discontinuities between the upper alluvial aquifer and the lower CH aquifer, suggesting that they are in hydraulic continuity. The hydraulic heads for both aquifers are

aligned as plotted in Fig. 1c. Piezometric heads range from 350–400, 320–340 and 295–320 m; computed hydraulic gradients of 2.5–5.5, 1–1.5 and 0.5–1 ‰ in the upstream part, central and downstream part of the GM basin, respectively. The general direction of groundwater flow is southeast to northwest at upstream, then east-west at downstream. This direction is the same as the flow of the RGM. Moreover, the piezometric contours in the valley show concave shapes, oriented in the direction of the river flow. These observations suggest replenishment of groundwater by focused recharge supplied by leakage from the ephemeral RGM.

5 Discussion

Geologically, the observed upstream-downstream transition in geophysical and hydrogeological properties may be related to paleo-sedimentary events. For example, lithological variations observed in the pebbly sands series of the CH and confirmed by the difference in resistivity within this formation, suggest that it was deposited during geological events of varying intensity. This deduction is consistent with the hypothesis of Greigert (1966), who suggested that deep alteration in the Upper Cretaceous and uplift of Antecambrian formations are responsible for the establishment of the pebbly sand series observed in Fig. 4, Fig. 6b and c, in an environment characterized by substantial relief and high energy surface flows.

The clay-sandstone series, newly highlighted in the downstream part of the study area (Fig. 4, Fig. 6c-d), is thought to have formed as transition facies between the continental Cretaceous essentially detrital formations of the Maradi region (Iullemmeden basin edge) and the marine Cretaceous clay-limestone formations located in the center of the Iullemmeden basin. Similarly, an identical transition series was demonstrated in the eastern part of Niger within the Iullemmeden basin (Faure, 1966).

A lithostratigraphic column summarizes the lithology, resistivity, and effective porosity of the various formations encountered in the study area (Fig. 7). For alluvial formations, their thicknesses range from 6 to 30 m, and their lithology varies from upstream to downstream. In the upstream part, they are composed of old and recent formations. Older alluvium comprises coarse sands with pebbles and is located at the top of the pebbly sands series of the CH with which they share similar resistivities and effective porosities (Fig. 6b-c). This observation is consistent with that found by BRGM (1978) suggesting that the older alluvium stems from the reworking of the CH pebbly sands series. In contrast, recent alluvium constituting the surface horizons of 0 to 10 m, is formed of clayey sands and clays, depending on the location. For example, in the Djirataoua site, borehole lithological logs suggest that recent alluvium consists of compact clays with a thickness of between 6 and 10 m. At this site, piezometric observations suggest that recent alluvium forms a confining layer of low permeability clays (see cross-section in Fig. 8). In the downstream part, the River GM has incised into the clay-sandstone series of the CH. The alluvium comprises fine clayey sands and sandy clay, which account for the low effective porosities and resistivities observed (Fig. 6d-e).

From our results, we realize a conceptual model representative of the RGMB (Fig. 9). Through the description of the results presented in section 4.4, we show that in the upstream part, the alluvium and the pebbly sand series of CH have a high MRS effective porosity, with a relatively long relaxation time (T_1), and medium to high electrical resistivities. These formations are considered porous and permeable. On the other hand, the clay-sandstone series and the Farak-type sandstones of CH formation downstream have low resistivities, effective porosity, and relaxation times. These changes indicate that the clay-sandstone formations are less permeable than the alluvium and pebble sandstones of CH. Additionally, the MRS effective porosity profiles do not show any discontinuities between the alluvium and the underlying CH formations. The groundwater flow

pattern suggests that groundwater is replenished by the focused recharge via leakage from the ephemeral RGM. As a result, we conclude that the aquifers are interconnected, except where inhibited by the surface geology (Djirataoua), and focused recharge via ephemeral river flow is transmitted to the underlying alluvial and CH aquifers.

Conclusions

The geometry and properties of an alluvium-bedrock aquifer system along the ephemeral River Goulbi de Maradi in the Iullemmeden basin of Niger are characterized by combined MRS-TDEM surface geophysical surveys and borehole lithological logs. We identify lithological variations from upstream to downstream in which effective porosity and resistivity decrease. Upstream, the shallow alluvial aquifer has an effective porosity ranging from 9 to 36% with a thickness of 6 to 15 m. Downstream in the rest of the valley, the alluvial aquifer deepens (25 to 30 m) with effective porosities ranging from 7 to 20%; resistivity values range from 12 to 57 Ω m upstream and 25 Ω m downstream. For the Continental Hamadien, three aquifer layers are revealed. Two upper layers are juxtaposed laterally: (i) a stony sands series upstream with 13 to 19% for the average effective porosity and 22 to 800 Ω m for the resistivity values; and (ii) a clay-sandstone series downstream with 3 to 10% effective porosity average and 10 to 43 Ω m for resistivity values. The Farak-type sandstones are located at the base of these formations with an average resistivity of 11 Ω m. MRS experiments indicate that the alluvial aquifer and underlying CH aquifer show continuous effective porosity profiles at depth, suggesting that they form an interconnected aquifer system that is replenished by focused groundwater recharge arising from leakage from the ephemeral River Goulbi de Maradi. The development of this conceptual model of the groundwater system in this Sahelian dryland is of vital importance given the dependence upon groundwater for drinking water, food supply and livelihoods from agriculture and industry.

Acknowledgments

The authors wish to acknowledge support from the GroFutures (Groundwater Futures in Sub-Saharan Africa) research project funded by the NERC-ESRC-DFID (UK) UPGro program (grant refs. NE/M008576/1, NE/M008932/1).

References

Abdou Babaye, M. S., Orban, P., Ousmane, B., Favreau, G., Brouyère, S., & Dassargues, A. (2019). Characterization of recharge mechanisms in a Precambrian basement aquifer in semi-arid south-west Niger. *Hydrogeology Journal*, *27*(2), 475–491. https://doi.org/10.1007/s10040-018-1799-x

Archie, G. E. (1941). *The Electrical Resistivity Log as an Aid in Determining Some Reservoir Characteristics*. (October), 54–62.

Barsukov, P. O., Fainberg, E. B., & Khabensky, E. O. (2015). Shallow Investigations by TEM-FAST Technique : Methodology and Examples. In *Electromagnetic Sounding of the Earth's Interior: Theory, Modeling, Practice* (Second Edi). https://doi.org/10.1016/B978-0-444-63554-9/00003-9

Behroozmand, A. A., Keating, K., & Auken, E. (2015). A Review of the Principles and Applications of the NMR Technique for Near-Surface Characterization. *Surveys in Geophysics*, *36*(1), 27–85. https://doi.org/10.1007/s10712-014-9304-0

Behroozmand, A., Auken, E., Fiandaca, G., & Christiansen, A. V. (2012). MRS Parameter Estimation – Improvement by Joint and Laterally Constrained Inversion of MRS and TEM Data. *Near Surface Geoscience 2012*, *77*(4). https://doi.org/10.3997/2214-4609.20143388

Bierkens, M. F. P., & Wada, Y. (2019). Non-renewable groundwater use and groundwater depletion: a review. *Environmental Research Letters*, *14*(6), 063002. https://doi.org/10.1088/1748-9326/ab1a5f

Boucher, M., Favreau, G., Vouillamoz, J. M., Nazoumou, Y., & Legchenko, A. (2009). Estimating specific yield and transmissivity with magnetic resonance sounding in an unconfined sandstone aquifer (Niger). *Hydrogeology Journal*, *17*(7), 1805–1815. https://doi.org/10.1007/s10040-009-0447-x

Boucher, Marie, Favreau, G., Descloitres, M., Vouillamoz, J.-M., Massuel, S., Nazoumou, Y., … Legchenko, A. (2009). Contribution of geophysical surveys to groundwater modelling of a porous aquifer in semiarid Niger: An overview. *Comptes Rendus Geoscience*, *341*(10–11), 800–809. https://doi.org/10.1016/j.crte.2009.07.008

Boucher, Marie, Favreau, G., Nazoumou, Y., Cappelaere, B., Massuel, S., & Legchenko, A. (2012). Constraining Groundwater Modeling with Magnetic Resonance Soundings. *Ground Water*, *50*(5), 775–784. https://doi.org/10.1111/j.1745-6584.2011.00891.x

BRGM. (1978). *Etudes comparatives du projet du Goulbi de Maradi : Evaluation et gestion des ressources en eaux souterraines du système des alluvions. Rapport BRGM 78 AGE 017*.

Calow, R. C., MacDonald, A. M., Nicol, A. L., & Robins, N. S. (2010). Ground Water Security and Drought in Africa: Linking Availability, Access, and Demand. *Ground Water*, *48*(2), 246–256. https://doi.org/10.1111/j.1745-6584.2009.00558.x

Carter, R. C., & Alkali, A. G. (1996). Shallow groundwater in the northeast arid zone of Nigeria. *Quarterly Journal of Engineering Geology and Hydrogeology*, *29*(4), 341–355.

https://doi.org/10.1144/GSL.QJEGH.1996.029.P4.07

Cooper, H. H., & Jacob, C. E. (1946). A generalized graphical method for evaluating formation constants and summarizing well-field history. *Transactions, American Geophysical Union*, *27*(4), 526. https://doi.org/10.1029/TR027i004p00526

Costa, A. C., Bronstert, A., & De Araújo, J. C. (2012). A channel transmission losses model for different dryland rivers. *Hydrology and Earth System Sciences*, *16*(4), 1111–1135. https://doi.org/10.5194/hess-16-1111-2012

Cuthbert, M. O., Acworth, R. I., Andersen, M. S., Larsen, J. R., McCallum, A. M., Rau, G. C., & Tellam, J. H. (2016). Understanding and quantifying focused, indirect groundwater recharge from ephemeral streams using water table fluctuations. *Water Resources Research*, *52*(2), 827–840. https://doi.org/10.1002/2015WR017503

Cuthbert, Mark O, Taylor, R. G., Favreau, G., Todd, M. C., Shamsudduha, M., Villholth, K. G., … Kukuric, N. (2019). Observed controls on resilience of groundwater to climate variability in sub-Saharan Africa. *Nature*, *572*(7768), 230–234. https://doi.org/10.1038/s41586-019-1441-7

Dahan, O., Tatarsky, B., Enzel, Y., Kulls, C., Seely, M., & Benito, G. (2008). Dynamics of Flood Water Infiltration and Ground Water Recharge in Hyperarid Desert. *Ground Water*, *46*(3), 450–461. https://doi.org/10.1111/j.1745-6584.2007.00414.x

Descloitres M., Chalikakis K., Legchenko A., Moussa A. M., Genthon P., Favreau G., Le Coz, M., Boucher, M., O. M. (2013). Investigation of groundwater resources in the Komadugu Yobe Valley (Lake Chad Basin, Niger) using MRS and TDEM methods. *Journal of African Earth*

Sciences, *87*, 71–85. https://doi.org/10.1016/j.jafrearsci.2013.07.006

Dikouma, M. (1990). Fluctuation du niveau marin au Maestrichtien et au Paléocène dans le bassin Intracratonique des Iullemmeden (Ader-Doutchi, Niger). *Thèse Doctorat, Univ. Dijon-Niamey*, 273p.

Durand A; Icole M; Bieda S. (1981). Sédiments et climats quaternaires du Sahel central : exemple de la vallée de Maradi (Niger méridional). *UNIV., SERVICE GEOL./NIAMEY/NER*, *VOL. 12*; *N*(January 1981).

Ezersky, M., Legchenko, A., Al-Zoubi, A., Levi, E., Akkawi, E., & Chalikakis, K. (2011). TEM study of the geoelectrical structure and groundwater salinity of the Nahal Hever sinkhole site, Dead Sea shore, Israel. *Journal of Applied Geophysics*, *75*(1), 99–112. https://doi.org/10.1016/j.jappgeo.2011.06.011

Faure, H. (1966). *Reconnaissance Géologiques des Formations Sedimentaires Post Paléozoiques du Niger Oriental, Direction des Mines et de la Géologie,(Niger). In Publication No. 1. Bur. Rech. Geol. Minieres Paris.*

Favreau, G, Cappelaere, B., Massuel, S., Leblanc, M., Boucher, M., Boulain, N., & Leduc, C. (2009). Land clearing, climate variability, and water resources increase in semiarid southwest Niger: A review. *Water Resources Research*, *45*(7), 1–18. https://doi.org/10.1029/2007WR006785

Favreau, G., Nazoumou, Y., Leblanc, M., Guéro, A., & Goni, I. B. (2012). Groundwater resources increase in the Iullemmeden Basin, West Africa. *In Climate Change Effects on Groundwater Resources: A Global Synthesis of Findings and Recommendations (Pp. 113-128). CRC Press.*

573 Flinchum, B. A., Banks, E., Hatch, M., Batelaan, O., Peeters, L. J. M., & Pasquet, S. (2020).
574 Identifying recharge under subtle ephemeral features in a flat-lying semi-arid region using a
575 combined geophysical approach. *Hydrology and Earth System Sciences*, *24*(9), 4353–4368.
576 https://doi.org/10.5194/hess-24-4353-2020

577 Gev, I., Goldman, M., Rabinovich, B., Rabinovich, M., & Issar, A. (1996). Detection of the water
578 level in fractured phreatic aquifers using nuclear magnetic resonance (NMR) geophysical
579 measurements. *Journal of Applied Geophysics*, *34*(4), 277–282. https://doi.org/10.1016/0926-
580 9851(96)00004-3

581 Goldman, M., Rabinovich, B., Rabinovich, M., Gilad, D., Gev, I., & Schirov, M. (1994).
582 Application of the integrated NMR-TDEM method in groundwater exploration in Israel.
583 *Journal of Applied Geophysics*, *31*(1–4), 27–52. https://doi.org/10.1016/0926-
584 9851(94)90045-0

585 Greigert, J. (1966). *Description des formations crétacées et tertiaires du bassin des Iullemmeden.*
586 *Rapport BRGM,Orléans, France*. 236.

587 Greigert, J. (1978). *Atlas des eaux souterraines de la République du Niger.Etat des*
588 *connaissances.Rapport BRGM_79 AGE001.Orléans_France.*

589 INS. (2012). *Recensement Général de la Population et de l'Habitat 2012*. (NER-INS-RGPH-2012-
590 V1.0). https://doi.org/http://anado.ins.ne/index.php

591 Issa Lélé, M., & Lamb, P. J. (2010). Variability of the Intertropical Front (ITF) and Rainfall over
592 the West African Sudan–Sahel Zone. *Journal of Climate*, *23*(14), 3984–4004.
593 https://doi.org/10.1175/2010JCLI3277.1

Issoufou Ousmane B. (2014). *Impact de l'irrigation et de la variabilité climatique sur la nappe alluviale du Goulbi Maradi : cas du périmètre irrigué de Djiratoua.* Univ. Abdou Moumouni Niamey.

Jasechko, S., & Perrone, D. (2021). Global groundwater wells at risk of running dry. *Science*, *372*(6540), 418–421. https://doi.org/10.1126/science.abc2755

Kafri, U., & Goldman, M. (2005). The use of the time domain electromagnetic method to delineate saline groundwater in granular and carbonate aquifers and to evaluate their porosity. *Journal of Applied Geophysics*, *57*(3), 167–178. https://doi.org/10.1016/j.jappgeo.2004.09.001

Kemgang Dongmo, T., Boucher, M., Mvondo, V. Y. E., Favreau, G., Ngounou Ngatcha, B., Yalo, N., Goni, I. B., Legchenko, A (2019). Contribution of time domain electromagnetic and magnetic resonance soundings to groundwater assessment at the margin of lake chad basin, cameroon. *Journal of Applied Geophysics*, *170*, 103840. https://doi.org/10.1016/j.jappgeo.2019.103840

Legchenko, A. (2007). MRS measurements and inversion in presence of EM noise. *Boletin Geologico y Minero*, *118*,(3).

Legchenko, A., Baltassat, J.-M., Bobachev, A., Martin, C., Robain, H., & Vouillamoz, J.-M. (2004). Magnetic Resonance Sounding Applied to Aquifer Characterization. *Ground Water*, *42*(3), 363–373. https://doi.org/10.1111/j.1745-6584.2004.tb02684.x

Legchenko, A., Baltassat, J. M., Beauce, A., & Bernard, J. (2002). Nuclear magnetic resonance as a geophysical tool for hydrogeologists. *Journal of Applied Geophysics*, *50*(1–2), 21–46. https://doi.org/10.1016/S0926-9851(02)00128-3

Legchenko, A., Ezersky, M., Camerlynck, C., Al-Zoubi, A., & Chalikakis, K. (2009). Joint use of TEM and MRS methods in a complex geological setting. *Comptes Rendus Geoscience*, *341*(10–11), 908–917. https://doi.org/10.1016/j.crte.2009.07.013

Legchenko, A., Miège, C., Koenig, L. S., Forster, R. R., Miller, O., Solomon, D. K., … Brucker, L. (2018). Estimating water volume stored in the south-eastern Greenland firn aquifer using magnetic-resonance soundings. *Journal of Applied Geophysics*, *150*, 11–20. https://doi.org/10.1016/j.jappgeo.2018.01.005

Legchenko, A. and Valla, P. (2002). A review of the basic principles for proton magnetic resonance sounding measurements. *Journal of Applied Geophysics*, *50*(1–2), 3–19. https://doi.org/10.1016/S0926-9851(02)00127-1

Legchenko, A., Vouillamoz, J., Lawson, F. M. A., Alle, C., Descloitres, M., & Boucher, M. (2016). Interpretation of magnetic resonance measurements in the varying earth's magnetic field. *Geophysics*, *81*(4), WB23–WB31. https://doi.org/10.1190/geo2015-0474.1

Lubczynski, M., & Roy, J. (2005). MRS contribution to hydrogeological system parametrization. *Near Surface Geophysics*, *3*(3), 131–139. https://doi.org/10.3997/1873-0604.2005009

MacDonald, A. M., Bonsor, H. C., Dochartaigh, B. É. Ó., & Taylor, R. G. (2012). Quantitative maps of groundwater resources in Africa. *Environmental Research Letters*, *7*(2), 024009. https://doi.org/10.1088/1748-9326/7/2/024009

Meier, P. M., Carrera, J., & Sánchez-Vila, X. (1998). An evaluation of Jacob's Method for the interpretation of pumping tests in heterogeneous formations. *Water Resources Research*, *34*(5), 1011–1025. https://doi.org/10.1029/98WR00008

636 Mignon, R. (1970). Étude géologique et prospection du Damagaram Mounio et du Sud Maradi.
637 *Rapport BRGM*, *70*, 46-51.

638 Nabighian M.N., Macnae, J.C . (1991). Time Domain Electromagnetic Methods. Electromagnetic
639 Methods in Applied Geophysics 2:Applications. SEG Publ., pp. 427–520 (chapter 6)

640 Nazoumou, Y., Favreau, G., Adamou, M. M., & Maïnassara, I. (2016). La petite irrigation par les
641 eaux souterraines, une solution durable contre la pauvreté et les crises alimentaires au Niger ?
642 *Cahiers Agricultures*, *25*(1), 15003. https://doi.org/10.1051/cagri/2016005

643 ORSTOM. (1972). *Note hydrologique sur le Goulbi de Maradi et le Lac de Madarounfa*. *Rapport*
644 *technique ORSTOM.*

645 OSS. (2008). Système aquifère d'Iullemeden (Mali, Niger, Nigeria): gestion concertée des
646 ressources en eau partagées d'un aquifère transfrontalier sahélien. *OSS*, (Rapport technique).

647 Plata, J. L., & Rubio, F. M. (2008). The use of MRS in the determination of hydraulic
648 transmissivity: The case of alluvial aquifers. *Journal of Applied Geophysics*, *66*(3–4), 128–
649 139. https://doi.org/10.1016/j.jappgeo.2008.04.001

650 Sánchez-Vila, X., Meier, P. M., & Carrera, J. (1999). Pumping tests in heterogeneous aquifers: An
651 analytical study of what can be obtained from their interpretation using Jacob's Method. *Water*
652 *Resources Research*, *35*(4), 943–952. https://doi.org/10.1029/1999WR900007

653 Scanlon, B. R., Faunt, C. C., Longuevergne, L., Reedy, R. C., Alley, W. M., McGuire, V. L., &
654 McMahon, P. B. (2012). Groundwater depletion and sustainability of irrigation in the US High
655 Plains and Central Valley. *Proceedings of the National Academy of Sciences of the United*
656 *States of America*, *109*(24), 9320–9325. https://doi.org/10.1073/pnas.1200311109

Scanlon, B. R., Keese, K. E., Flint, A. L., Flint, L. E., Gaye, C. B., Edmunds, W. M., & Simmers, I. (2006). Global synthesis of groundwater recharge in semiarid and arid regions. *Hydrological Processes*, *20*(15), 3335–3370. https://doi.org/10.1002/hyp.6335

Schirov, M., Legchenko, A., & Creer, G. (1991). A new direct non-invasive groundwater detection technology for Australia. *Exploration Geophysics*, *22*(2), 333–338. https://doi.org/10.1071/EG991333

Seddon, D., Kashaigili, J.J., Taylor, R.G., Cuthbert, M.O., Mwihumbo, C. and MacDonald, A.M., 2021. Focused groundwater recharge in a tropical dryland: empirical evidence from central, semi-arid Tanzania. *Journal of Hydrology - Regional Studies*, Vol. 37, 100919. https://doi.org/10.1016/j.ejrh.2021.100919

Siebert, S., Burke, J., Faures, J. M., Frenken, K., Hoogeveen, J., Döll, P., & Portmann, F. T. (2010). Groundwater use for irrigation – a global inventory. *Hydrology and Earth System Sciences*, *14*(10), 1863–1880. https://doi.org/10.5194/hess-14-1863-2010

Taylor, R.G., Koussis, A. D., & Tindimugaya, C. (2009). Groundwater and climate in Africa—a review. *Hydrological Sciences Journal*, *54*(4), 655–664. https://doi.org/10.1623/hysj.54.4.655

Taylor, R.G., Scanlon, B., Döll, P., Rodell, M., Van Beek, R., Wada, Y., … Treidel, H. (2013). Ground water and climate change. *Nature Climate Change*, *3*(4), 322–329. https://doi.org/10.1038/nclimate1744

Toyin, A., Adekeye, O. A., Bale, R. B., Sanni, Z. J., & Jimoh, O. A. (2016). Lithostratigraphic description, sedimentological characteristics and depositional environments of rocks

penetrated by Illela borehole, Sokoto Basin, NW Nigeria: A connection between Gulf of Guinea Basins. *Journal of African Earth Sciences*, *121*, 255–266. https://doi.org/10.1016/j.jafrearsci.2016.06.011

Villeneuve, S., Cook, P. G., Shanafield, M., Wood, C., & White, N. (2015). Groundwater recharge via infiltration through an ephemeral riverbed, central Australia. *Journal of Arid Environments*, *117*, 47–58. https://doi.org/10.1016/j.jaridenv.2015.02.009

Vouillamoz, J.-M., Hoareau, J., Grammare, M., Caron, D., Nandagiri, L., & Legchenko, A. (2012). Quantifying aquifer properties and freshwater resource in coastal barriers: a hydrogeophysical approach applied at Sasihithlu (Karnataka state, India). *Hydrology and Earth System Sciences*, *16*(11), 4387–4400. https://doi.org/10.5194/hess-16-4387-2012

Vouillamoz, J. M., Descloitres, M., Toe, G., & Legchenko, A. (2005). Characterization of crystalline basement aquifers with MRS: comparison with boreholes and pumping tests data in Burkina Faso. *Near Surface Geophysics*, *3*(3), 205–213. https://doi.org/10.3997/1873-0604.2005015

Vouillamoz, J. M., Favreau, G., Massuel, S., Boucher, M., Nazoumou, Y., & Legchenko, A. (2008). Contribution of magnetic resonance sounding to aquifer characterization and recharge estimate in semiarid Niger. *Journal of Applied Geophysics*, *64*(3–4), 99–108. https://doi.org/10.1016/j.jappgeo.2007.12.006

Vouillamoz, J. M., Lawson, F. M. A., Yalo, N., & Descloitres, M. (2015). Groundwater in hard rocks of Benin : Regional storage and buffer capacity in the face of change. *Journal of Hydrology*, *520*, 379–386. https://doi.org/10.1016/j.jhydrol.2014.11.024

699 Vouillamoz, J. M., Legchenko, A., & Nandagiri, L. (2011). Characterizing aquifers when using
700 magnetic resonance sounding in a heterogeneous geomagnetic field. *Near Surface*
701 *Geophysics*, *9*(2), 135–144. https://doi.org/10.3997/1873-0604.2010053

702 Vouillamoz, J. M. M., Lawson, F. M. A. M. A., Yalo, N., & Descloitres, M. (2014). The use of
703 magnetic resonance sounding for quantifying specific yield and transmissivity in hard rock
704 aquifers: The example of Benin. *Journal of Applied Geophysics*, *107*, 16–24.
705 https://doi.org/10.1016/j.jappgeo.2014.05.012

706 Wada, Y., van Beek, L. P. H., & Bierkens, M. F. P. (2012). Nonsustainable groundwater sustaining
707 irrigation: A global assessment. *Water Resources Research*, *48*(6).
708 https://doi.org/10.1029/2011WR010562

709 Wada, Y., van Beek, L. P. H., van Kempen, C. M., Reckman, J. W. T. M., Vasak, S., & Bierkens,
710 M. F. P. (2010). Global depletion of groundwater resources. *Geophysical Research Letters*,
711 *37*(20), n/a-n/a. https://doi.org/10.1029/2010GL044571

712 Wheater, H., Mathias, S., & Li, X. (2010). Groundwater modelling in arid and semi-arid areas. In
713 *Groundwater Modelling in Arid and Semi-Arid Areas* (Vol. 9780521111294).
714 https://doi.org/10.1017/CBO9780511760280

715 Zarate, E., Hobley, D., MacDonald, A. M., Swift, R. T., Chambers, J., Kashaigili, J. J., … Cuthbert,
716 M. O. (2021). The role of superficial geology in controlling groundwater recharge in the
717 weathered crystalline basement of semi-arid Tanzania. *Journal of Hydrology: Regional*
718 *Studies*, *36*, 100833. https://doi.org/10.1016/j.ejrh.2021.100833

719 **Figures List**

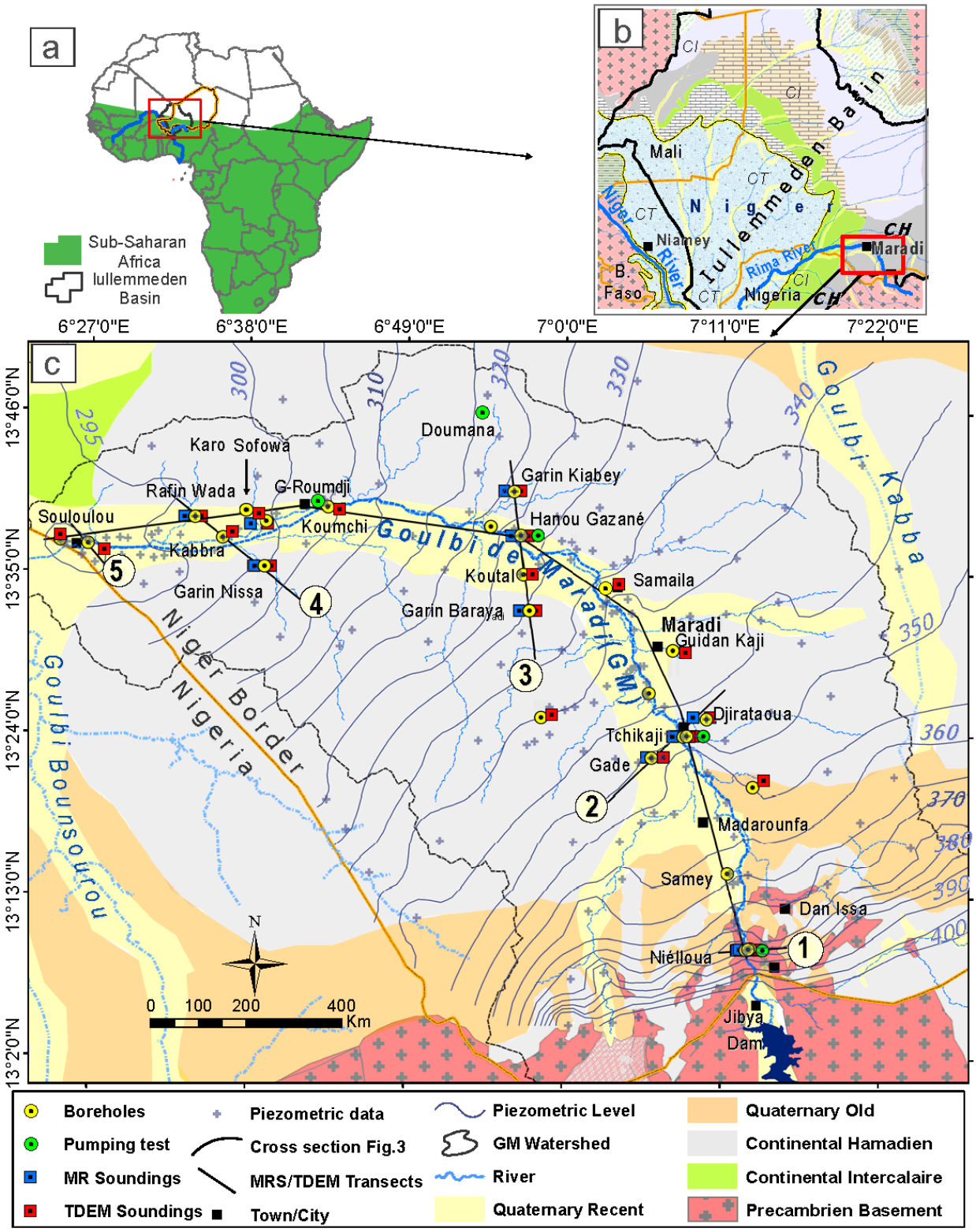

Fig. 1. Map location of study area: (**a**) map of Africa showing Sub-Saharan Africa and location of Iullemmeden basin (**b**) geological map of the Iullemmeden Basin, (**c**) map of the River Goulbi de Maradi Basin.

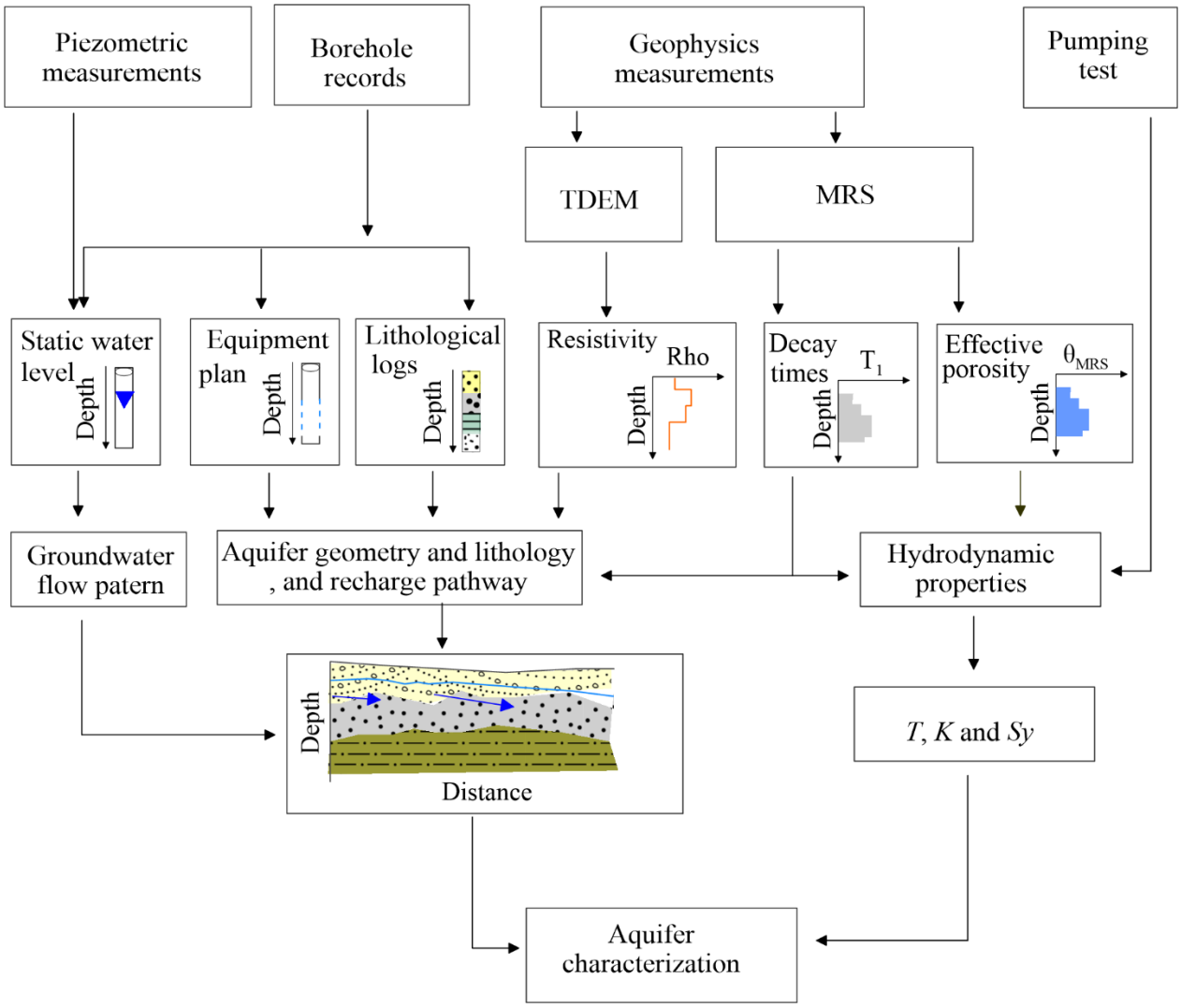

724

725 Fig. 2. Flow chart outlining the methodological approach employed in the study.

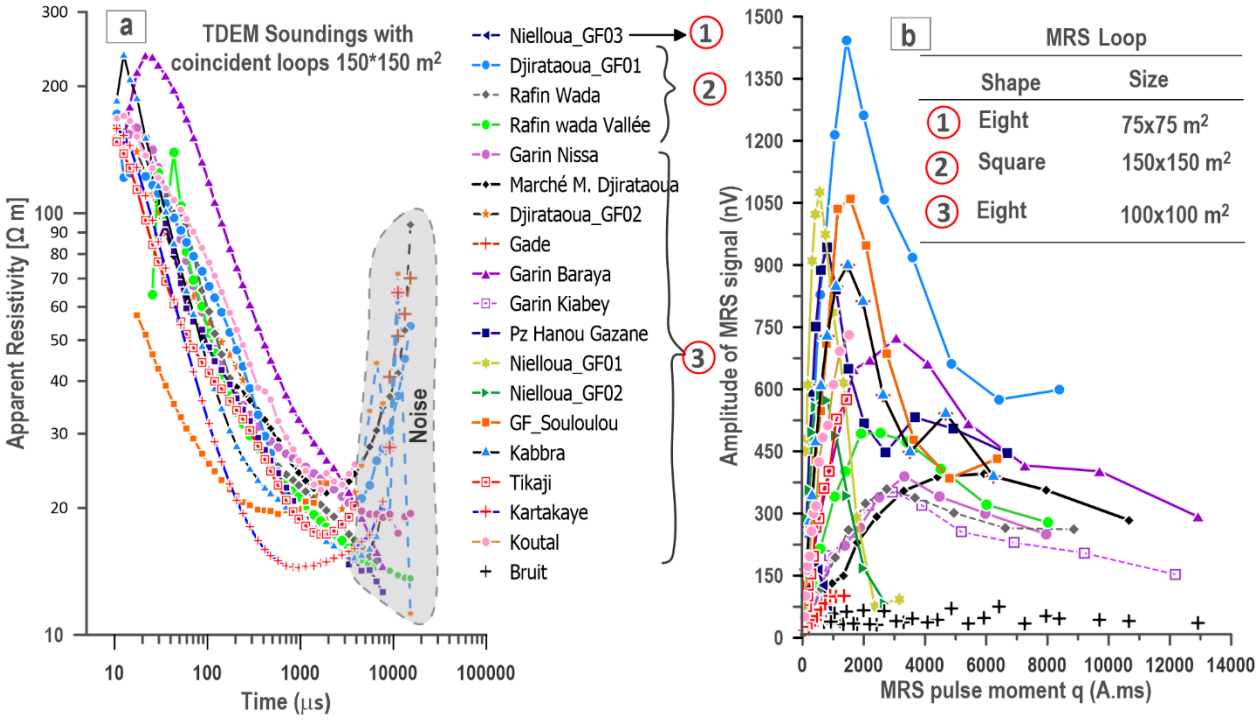

726

727 Fig. 3. Geophysical signals (raw field data): (**a**) TDEM apparent resistivity as a function of time,

728 (**b**) MRS amplitude as a function of pulse moment.

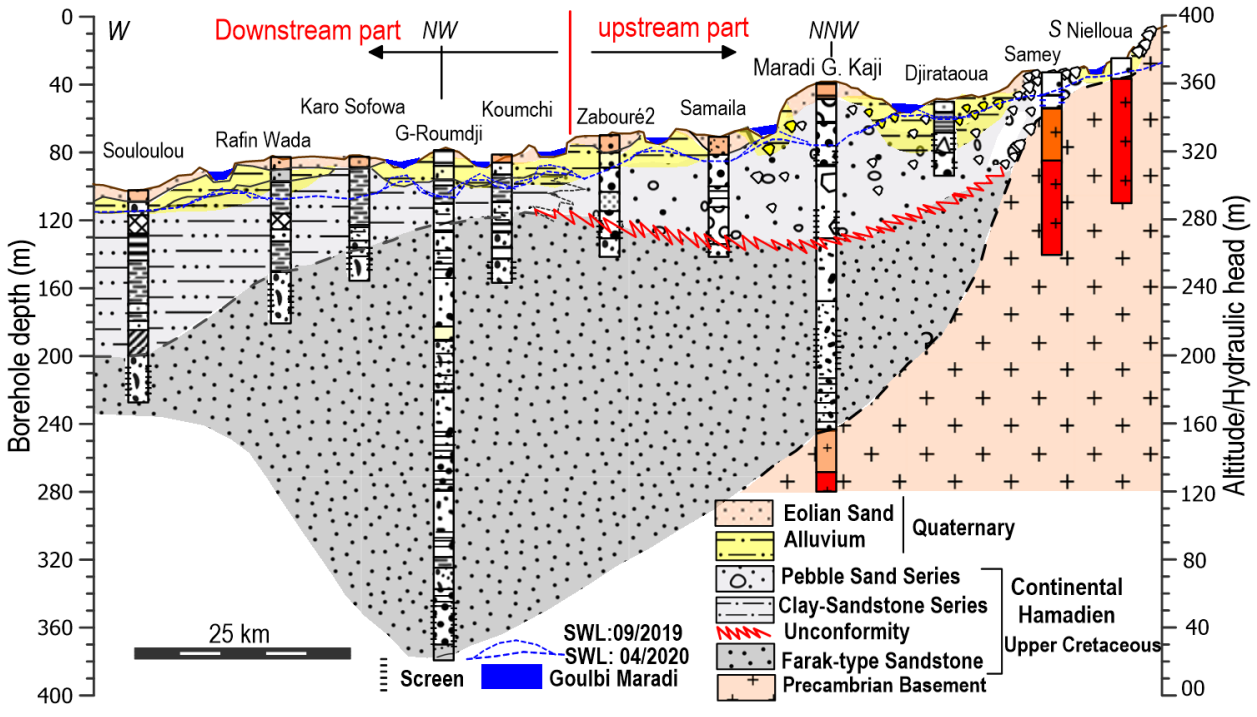

729

730 Fig. 4. Upstream-downstream hydrogeological cross-section.

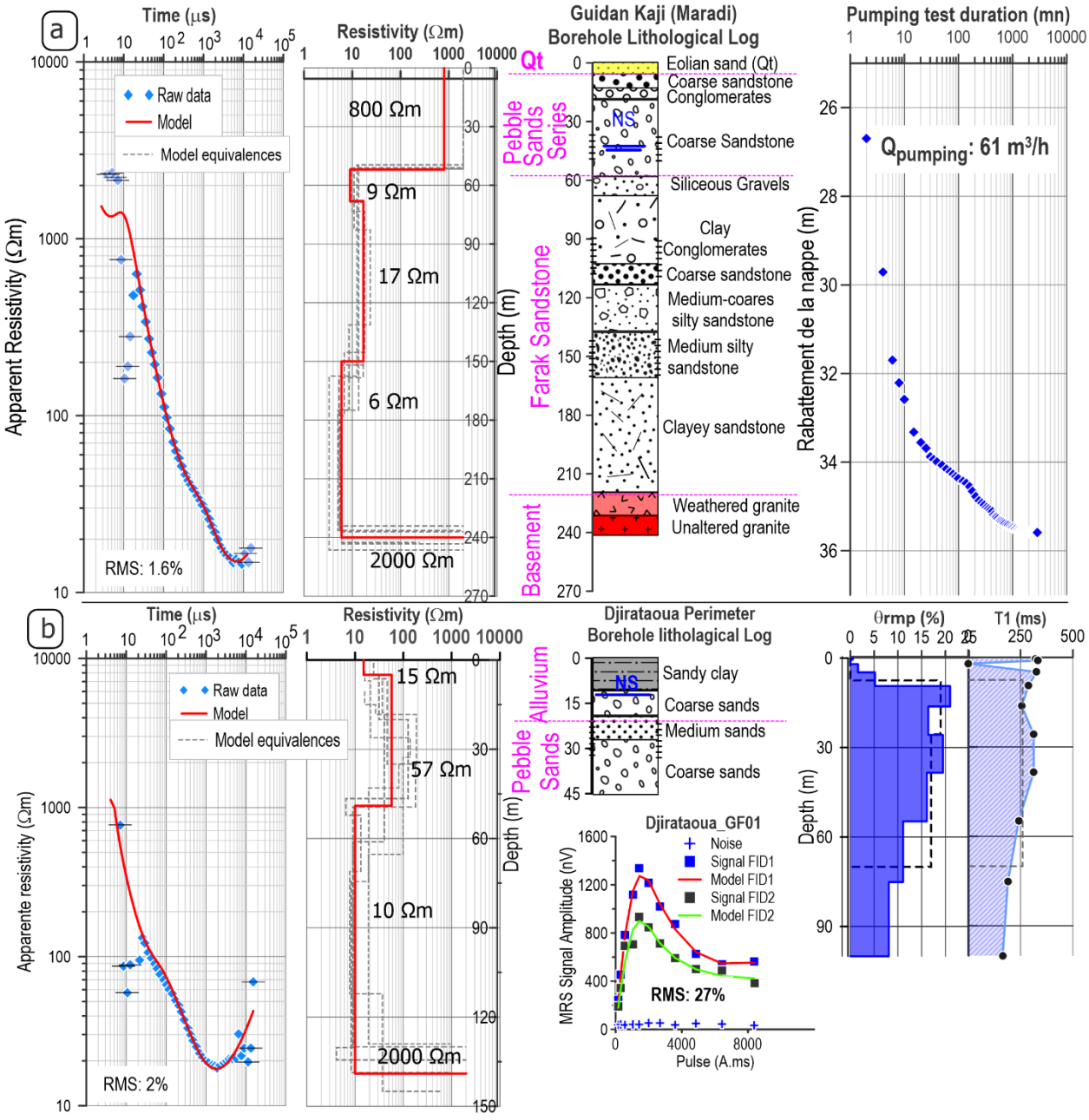

731

732 Fig. 5. Typical example of geophysical results of Guidan Kaji (**a**) and Djirataoua-GF01 (**b**) sites.
733 (**a**) From left to right: TDEM data, TDEM inversion, lithological section, and pumping test data.
734 (**b**) From the right to the left: TDEM data, TDEM inversion, lithological section, MRS data,
735 distribution of MRS water content and decay time T_1 as a function of depth.

736 (a) Transects 1 :

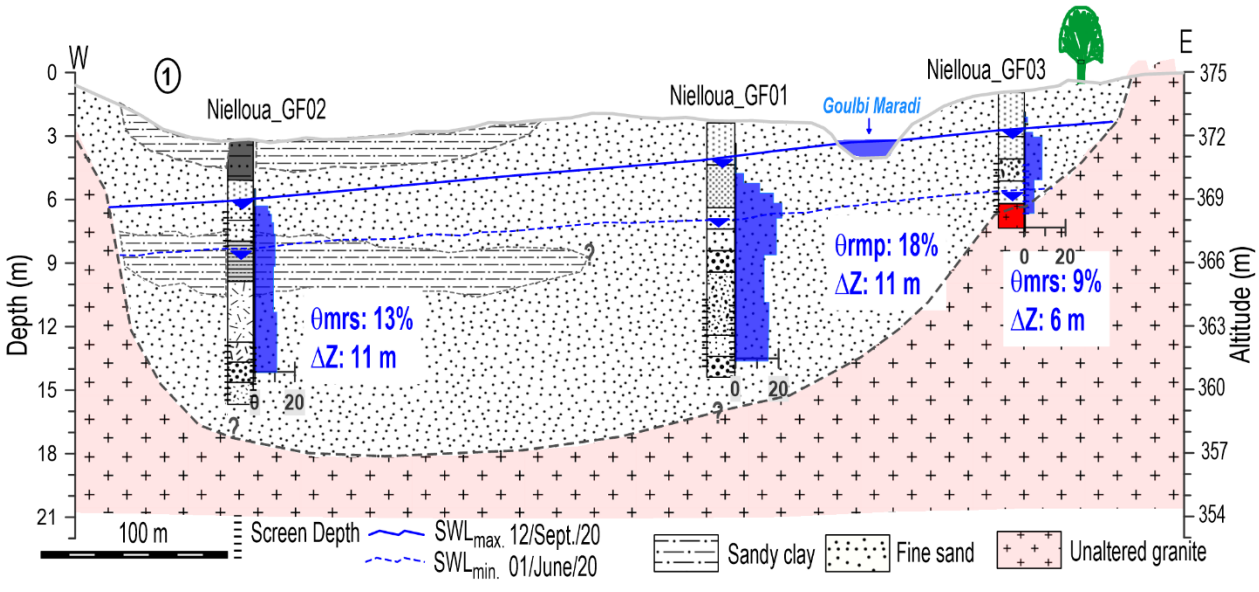

737

738 (b) Transects 2 :

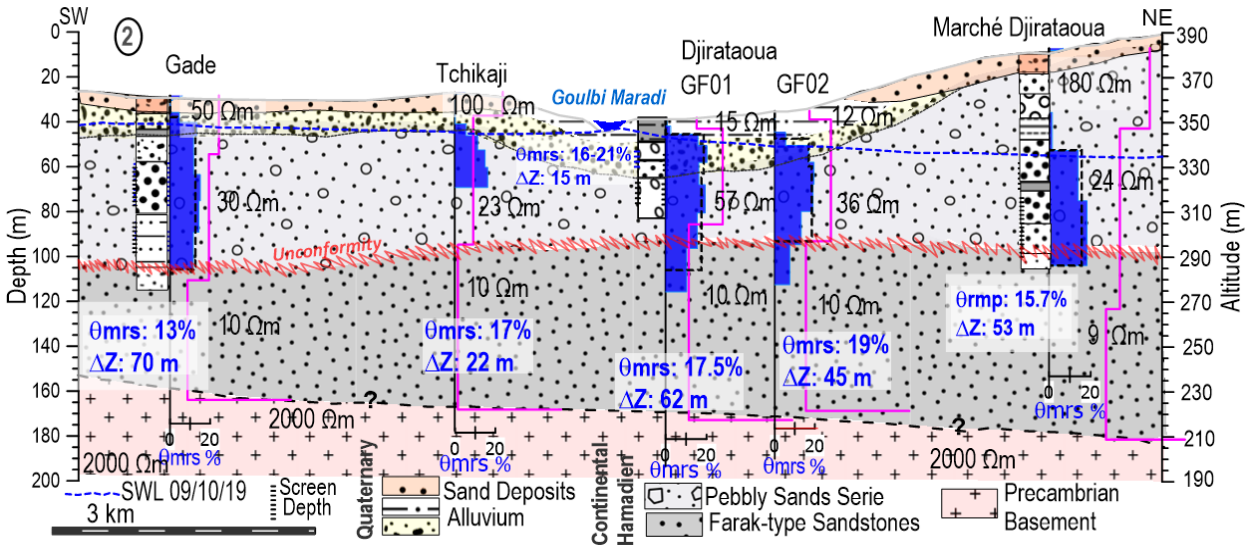

739

740 (c) Transects 3 :

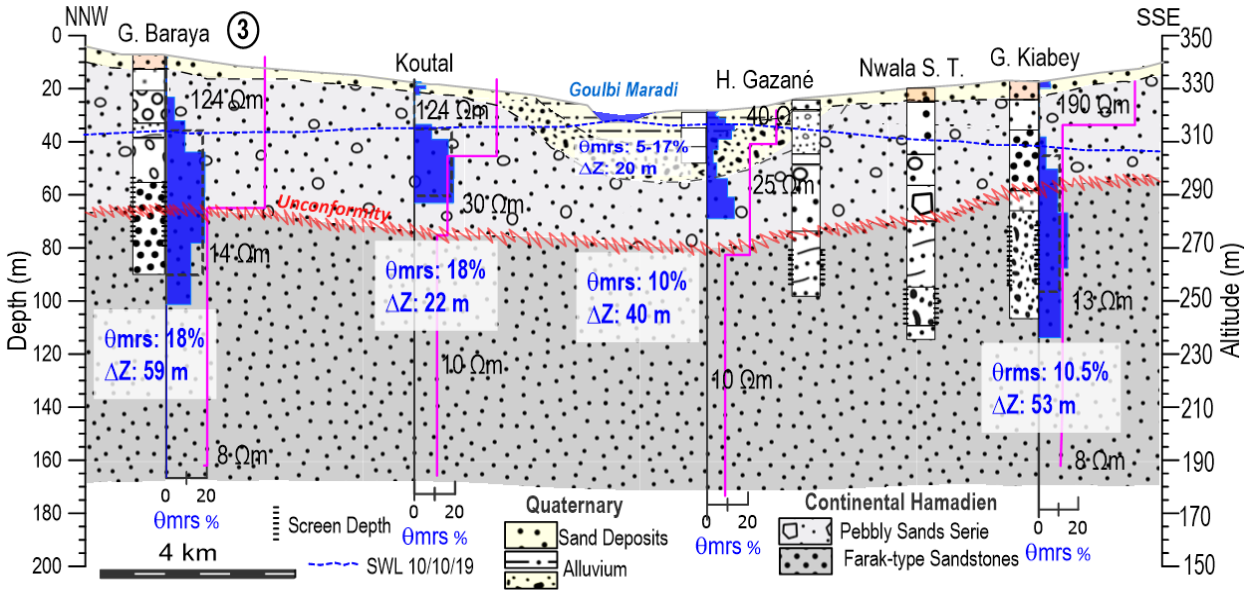

741

742 (d) Transect 4 :

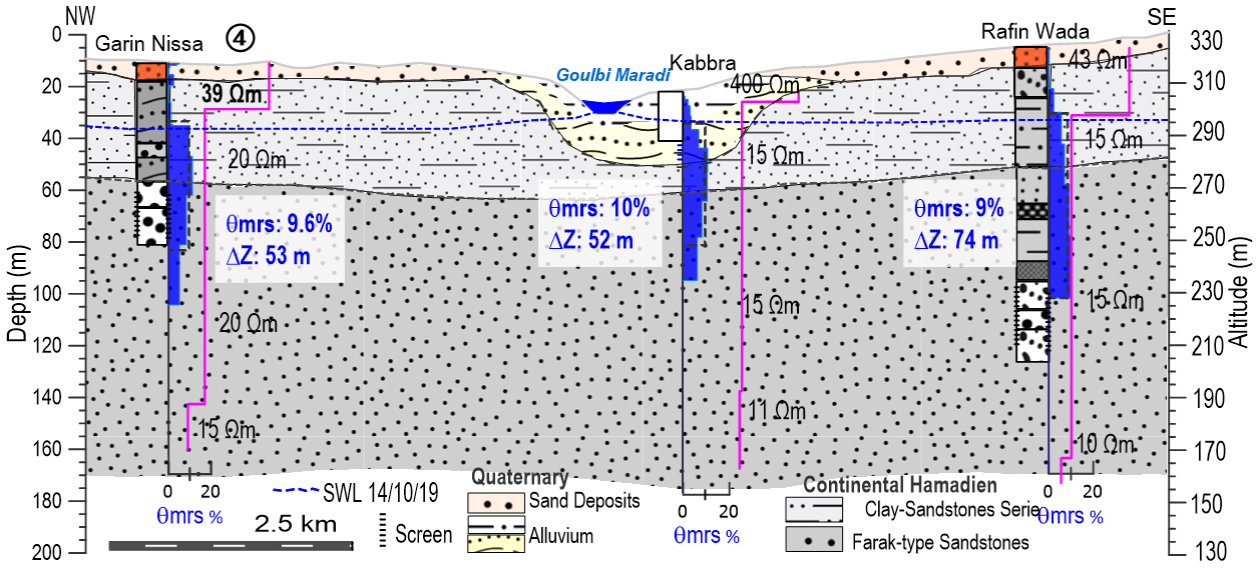

743

744 (e) Transects 5 :

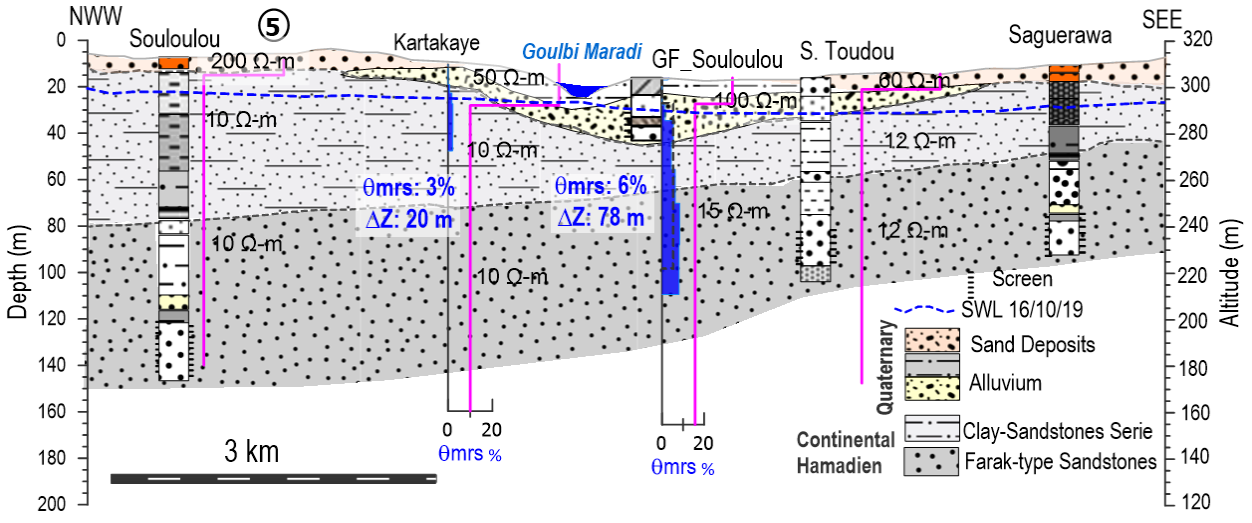

745

746 Fig. 6. MRS, TDEM, and borehole lithology results presented with topography.

Period		Group	MRS Water Content (%)	TDEM Resistivity (Ω.m)	Geological Units	Max Depth /Thickness (m)	Lithology	Env. deposit
Quaternary			6 - 18	12 - 57	Alluvium/Dune Sand	0		Fluvial/Aeolian
Upper Cretaceous	Upper Cenomanian	Continental Hamadien	10 - 17 / 3 - 10 / 10 - 43 / 22 - 800		Clay-sandstones / Pebbly Sands Serie	50 / 100		Continental / Unconformity
	Lower Cenomanian		6 - 17	~ 11	Farak Type Sandstones	150 / 200 / 250 / 300 / 350 / 400		Continental
Precambrian			--	~ 2000	Granite Basement	450 m		

747

748 Fig. 7. Lithostratigraphic column of the study area from geophysical result and borehole data
749 analysis.

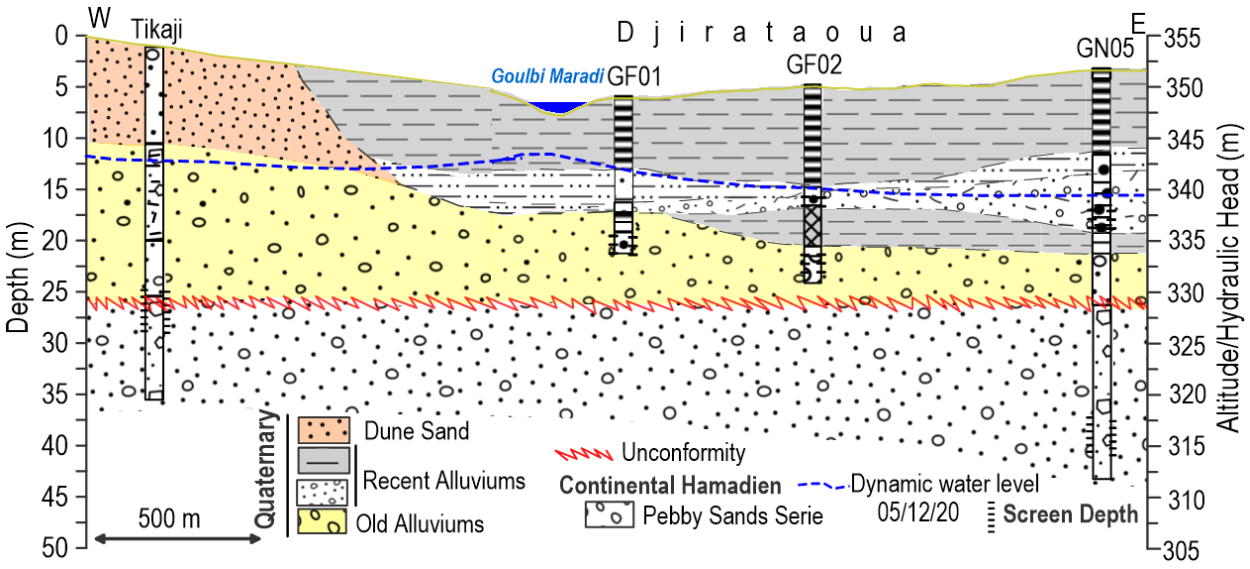

750

751 Fig. 8. Hydrogeological cross-section of the major bed of the Goulbi de Maradi River in

752 Djirataoua.

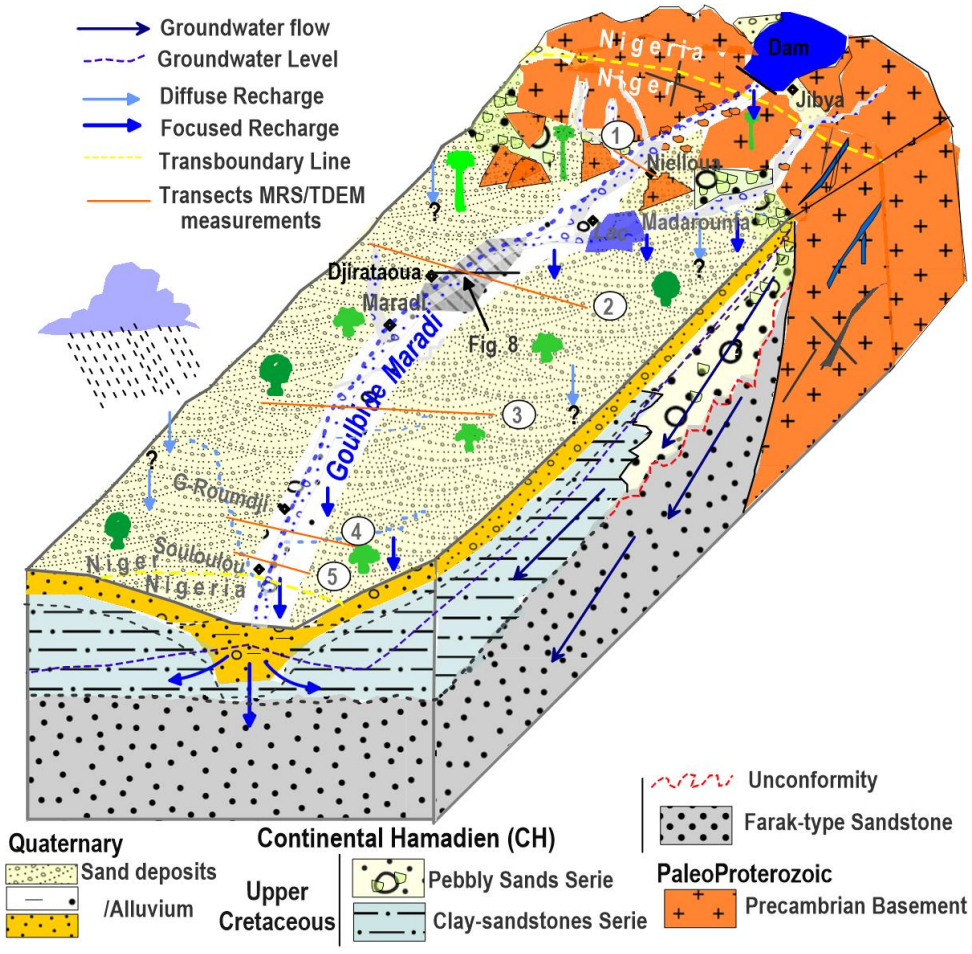

753

754 Fig. 9. Conceptual model of the transboundary valley of Goulbi de Maradi basin.

755 **Table lists**

756 Table 1

757 Characteristics of MRS soundings in the Goulbi de Maradi valley

Site	Numis Equip-Ment	Shape/Size MRS Loop	Puls Number	Stacking Average	S/N	Lat (°N)	Long (°E)	Date
Nielloua_GF01	Auto	Eight 50 m	12	190	09.2	13.1583	7.2152	12/02/21
Nielloua_GF02	Auto	Eight 37.5 m	10	146	10.1	13.1576	7.2121	11/02/21
Nielloua_GF03	Plus	Eight 75 m	10	370	04.6	13.1590	7.2172	13/01/19
Djirataoua_GF01	Plus	Square 150 m	11	145	29.5	13.3996	7.1380	14/01/19
Djirataoua_GF02	Plus	Eight 100 m	12	190	12.2	13.4005	7.1420	14/01/19
Tikaji	Auto	Eight 100 m	14	257	06.8	13.3961	7.1253	08/04/20
Gade	Plus	Eight 100 m	13	114	26.9	13.3757	7.1010	19/01/19
Marché Djirataoua	Plus	Eight 100 m	11	200	06.6	13.4198	7.1649	15/01/19
Pz_Hanou Gazané	Auto	Eight 100 m	14	150	16.4	13.6268	6.9483	16/02/21
Garin Baraya	Plus	Eight 100 m	11	178	13.7	13.5418	6.9586	17/01/19
Garin kiabey	Plus	Eight 100 m	12	165	08.7	13.6766	6.9402	18/01/19
Rafin Wada	Plus	Square 150 m	11	320	10.9	13.6455	6.5695	19/01/19
Rafin Wada Vallée	Plus	Square 150 m	11	114	15.9	13.6222	6.5972	18/01/19
Garin Nissa	Plus	Square 150 m	11	184	12.9	13.5900	6.6503	20/01/19
Kabbra	Plus	Eight 100 m	12	150	14.9	13.6216	6.6030	09/07/19
GF_Souloulou	Plus	Eight 100 m	12	200	08.7	13.6158	6.4480	10/07/19
Kartakaye	Auto	Eight 100 m	16	200	02.8	13.6228	6.4445	11/04/20
Koutal	Auto	Eight 100 m	16	203	09.1	13.5812	6.9518	10/04/20

Zagon Bahochi	Auto	Eight 100 m	10	250	--	13.5930	6.4542	10/04/20

758

759 Table 2

760 Pumping tests characteristics

Pumping Well	AEP Nielloua	AEP_Hanou Gazané	Djirataoua GN05	Guidan Kaji	Doumana	Guidan Roumdji
Observation Well	Nielloua GF02	GF_Hanou Gazané	Djirataou_Pz	---	---	---
Radial distance (m)	19	16	17	---	---	---
Pumping rate (m^3/h)	10	8.9	20	63	12	16
Pumping Duration	6	7	24	48	24	20
Recovery duration (h)	4.6	18	--	06	08	03
Drawdown (m)	0.3	01	--	35	2.6	6.5

761

762 Table 3

763 TDEM results according to geology

Geological formations	Max [Ω m]	Min [Ω m]	Average [Ω m]	Median [Ω m]	Standard deviation [Ω m]
Alluvium	57	12	31	30	17
Pebbly sands serie	800	22	132	70	208.3
Clay-sandstones serie	43	10	17.5	15	10.8
Farak-sandstones	17	06	11	10	2.8
Precambrian Basement	2000	2000	2000	2000	-

764

765 Table 4

766 MRS results according to geology

	Pebbly sand series + Farak-sandstones		Clay-sandstones series + Farak-sandstones		Alluvium	
	θ (%)	T_1 (ms)	θ (%)	T_1 (ms)	θ (%)	T_1 (ms)
Max	17.8	390	10.9	260	36	300
Min	10.5	220	03	180	07	220
Average	14	302	8.3	230	16.6	245
Median	15	315	09	240	15	315

St. deviation	2.7	50		2.9	36		09	28

767

768 Table 5

769 Pumping tests hydrodynamic properties.

Observation Well/ Pumping	Q_P (m^3/h)	t_p (h)	T_r (h)	T_P (m^2/s)	T_r (m^2/s)	Date
Nielloua_GF02	10	6	4.67	$2.2 \cdot 10^{-3}$	$4.7 \cdot 10^{-3}$	11/08/2019
GF_Hanou Gazané	8.9	7	18	$1.4 \cdot 10^{-3}$	$1.3 \cdot 10^{-3}$	14/08/2019
Djirataoua_GN05	20	24	--	$2.2 \cdot 10^{-2}$	--	17/09/2004
Guidan Kaji	63	48	--	$2.8 \cdot 10^{-3}$	--	14/02/2016
Doumana	13	24	--	$1.7 \cdot 10^{-3}$	--	08/04/2018
Guidan Roumdji	16	20	--	$2.0 \cdot 10^{-3}$	--	15/06/2019

770 Q_p Pumping rate (m^3/s); t_p Pumping duration (s); T_p Transmissivity during the pumping phase
771 (m^2/s); T_r Transmissivity during recovery phase.

772 Table 6

773 Boreholes data used for MRS calibration and static water level (*SWL*), and the MRS data are
774 effective porosity (θ), thickness of the saturated aquifer (Δz), static water level (SWL),
775 parametrization factor (*Cp*), transmissivity (*T*), Specific yield (*Sy*) and hydraulic conducitvity (*K*)

Site	Boreholes					MRS							
	Formation	smax (m)	Tpt (10-3m^2/s)	Sypt (%)	SLW (m)	SLW (m)	Cp (10^{-8}m/s/ms^2)	Δz (m)	θMRS (%)	T1 (ms)	TMRS (10^{-4} m^2/s)	KMRS (10^{-4} m/s)	SyMRS (%)
Nielloua_GF01	AGM				3.02	1.5		09	18	220	34	3.8	13.7
Nielloua_GF02	AGM	0.4	4.7	0.79	3.6	2.36	4.5	11	13	230	2.3	2.1	6.8
Nielloua_GF03	AGM				3.86	2.36		06	09	240	0.68	1.1	3.4
Djirataoua_GF01	AGM/CH				8.79	7.16		62	17.5	260	16	2.6	6.5
Djirataoua_GF02	AGM/CH	5.83	22		10.78	12.8	3	45	19	220	9	2	7.2
Marché Djirataoua	CH				47.0	47.0		53	15.7	380	26	4.9	6
Tikaji	CH				-	20.18		22	17	320	8.3	3.9	6.5
Gade	CH				14.0	10.14		70	13	250	12	1.8	4.9
Garin Kiabey	CH				30.2	29.0		53	10.5	300	11	2.1	4
Garin Baraya	CH				27.85	25.53		59	18	390	35	5.9	6.8
H-Gazane	AGM/CH	1.03	1.3	0.056	6.15	04.5	0.3	55	13	230	9.7	1.5	4.9
Koutal	CH				18.2	16.4		22	18	320	8.8	4	6.8
Kabbra	AGM/CH				14.65	13.26		52	10	240	6.5	1.3	3.8
Garin Nissa	CH				28.7	24.0		53	9.6	240	6.4	1.2	3.6
Rafin Wada	CH				25.16	26.3		60	09	260	8	1.3	3.4
Rafin Wada Vallé	AGM/CH				17.4	17.0		60	10.2	240	7.7	1.3	3.9
Kartakaye	CH				-	16.5		20	03	190	0.47	0.24	1.1
GF_Souloulou	AGM/CH				15.12	11.7		78	06	190	3.7	4.7	2.3